

Nematic State of the Pnictides Stabilized by the Interplay Between Spin, Orbital, and Lattice Degrees of Freedom

Shuhua Liang,^{1,2} Adriana Moreo,^{1,2} and Elbio Dagotto^{1,2}

¹*Department of Physics and Astronomy, University of Tennessee, Knoxville, TN 37966, USA*

²*Materials Science and Technology Division, Oak Ridge National Laboratory, Oak Ridge, TN 37831, USA*

(Dated: October 12, 2021)

The nematic state of the iron-based superconductors is studied in the undoped limit of the three-orbital (xz , yz , xy) spin-fermion model via the introduction of lattice degrees of freedom. Monte Carlo simulations show that in order to stabilize the experimentally observed lattice distortion and nematic order, and to reproduce photoemission experiments, *both* the spin-lattice and orbital-lattice couplings are needed. The interplay between their respective coupling strengths regulates the separation between the structural and Néel transition temperatures. Experimental results for the temperature dependence of the resistivity anisotropy and the angle-resolved photoemission (ARPES) orbital spectral weight are reproduced by the present numerical simulations.

PACS numbers: 74.70.Xa, 74.25.-q, 71.10.Fd

Introduction.- The discovery of high temperature superconductivity in the iron-based pnictides and selenides has provided a novel playground where several simultaneously active degrees of freedom (d.o.f.) determine the complex properties of these materials [1, 2]. The mechanism that leads to superconductivity in these compounds will only be fully understood once the spin, orbital, lattice, and charge are all together considered in a consistent theory. The parent compounds of most pnictides become antiferromagnetic (AFM) at a Néel temperature T_N where long-range collinear spin order develops with wavevector $(\pi, 0)$ in the iron sublattice notation [2] breaking rotational symmetry from C_4 to C_2 . This state is also characterized by an orthorhombic (\mathcal{O}_{rth}) lattice distortion with the longer (shorter) lattice constant along the AFM [ferromagnetic (FM)] direction and by the ferro-order of the d_{xz} and d_{yz} orbitals that otherwise would be degenerate [1]. In materials such as the undoped 122 compounds, the structural and magnetic transitions occur at the same temperature. However, neutron studies performed on $\text{LaO}_{1-x}\text{F}_x\text{FeAs}$ [2] indicate that the AFM transition can be preceded by a structural transition at a temperature $T_S > T_N$ [3, 4].

There are two main proposals to explain these results: (i) In one scenario, the magnetic interactions play the key role [5–9]. In this context the “nematic” state [10] at T_S is induced by breaking the Z_2 symmetry that links the otherwise degenerate $(\pi, 0)$ and $(0, \pi)$ collinear states, while at T_N the remaining $O(3)$ symmetry is broken. However, explicit Monte Carlo (MC) calculations using purely spin models [11, 12] revealed only a tiny difference between the two critical temperatures. This suggests that other d.o.f. may be needed to reinforce the nematicity mechanism since recent experiments revealed a nematic transition well above T_N for BaFe_2As_2 [13] and NaFeAs [14] that persists into the doped regime far from magnetic transitions. (ii) In another scenario, orbital fluctuations are the crucial component [15–21], sim-

ilarly as in the manganites where orbital order occurs well above the magnetic critical temperatures [22].

Both approaches explain some of the experimental data, but in practice it is difficult to disentangle the “driver” and “passenger” roles of the different d.o.f. The electron acoustic-phonon coupling responsible for standard tetragonal-orthorhombic structural transitions naively appears ruled out as a relevant d.o.f. because $\delta = [(a_x - a_y)/(a_x + a_y)] \approx 0.003$ in the pnictides [19, 20, 23] (a_x, a_y =lattice constants), and this δ is considered too small to produce the sizable anisotropies experimentally observed [13, 23].

The purpose of this Letter is to revisit the influence of the lattice d.o.f. in the pnictides via its introduction into the spin-fermion (SF) model for these materials [24–26]. This model phenomenologically considers the growing body of experimental evidence that requires a mixture of itinerant and localized d.o.f. to properly address the iron superconductors [2, 27, 28]. Here the itinerant sector will involve electrons in the xz , yz , and xy d -orbitals [29]. The localized spins represent the spin of the other d -orbitals [24, 25] or alternatively, in a Landau-Ginzburg context, the magnetic order parameter. To our knowledge this is the first time that all these ingredients are simultaneously studied, and the complexity of the problem requires a computational analysis. Moreover, our numerical approach also allows us to study temperatures above T_S where all d.o.f. develop only short-range fluctuations [7, 30], a regime difficult to reach by standard mean-field procedures. Our main result is that a complete description of the phenomenology of the undoped Fe-based superconductors requires the simultaneous presence of both the spin- and orbital-lattice couplings, suggesting a degree of complexity in these materials that was not previously anticipated.

Model and Method.- The lattice SF model considered here is based on the purely electronic model studied before [24–26] supplemented by the coupling to the lattice:

$$H_{\text{SF}} = H_{\text{Hopp}} + H_{\text{Hund}} + H_{\text{Heis}} + H_{\text{SL}} + H_{\text{OL}} + H_{\text{Stiff}}. \quad (1)$$

This (lengthy) full Hamiltonian is written explicitly in the Supplementary Material. H_{Hopp} is the Fe-Fe hopping of electrons with the amplitudes selected in previous publications to reproduce ARPES results [the specific hopping amplitudes used here can be read in Eqs.(1-3) and Table 1 of Ref. [29]]. The average number of electrons per itinerant orbital is $n=4/3$ [29]. Our focus on the undoped case is justified: this limit already contains the physics under discussion, calculations are simpler than for the doped case, and the quenched disordering effect of chemical doping is avoided. The Hund interaction is canonical: $H_{\text{Hund}} = -J_{\text{H}} \sum_{\mathbf{i}, \alpha} \mathbf{S}_{\mathbf{i}} \cdot \mathbf{s}_{\mathbf{i}, \alpha}$, with $\mathbf{S}_{\mathbf{i}}$ ($\mathbf{s}_{\mathbf{i}, \alpha}$) the localized (itinerant with orbital index α) spin. H_{Heis} is the Heisenberg interaction among the localized spins involving nearest-neighbors (NN) and next-NN interactions with couplings J_{NN} and J_{NNN} , respectively, and a ratio $J_{\text{NNN}}/J_{\text{NN}}=2/3$ [26] that favors collinear order (any value larger than 1/2 would have been equally effective).

Our emphasis will be on the coupling of spin and orbital with the structural transition. Within the spin-driven scenario, the state between T_N and T_S is characterized by short-range spin correlations $\Psi_{\mathbf{i}} = \mathbf{S}_{\mathbf{i}} \cdot \mathbf{S}_{\mathbf{i}+\mathbf{x}} - \mathbf{S}_{\mathbf{i}} \cdot \mathbf{S}_{\mathbf{i}+\mathbf{y}}$ that satisfy $\langle \Psi \rangle < 0$ [9], where $\mathbf{S}_{\mathbf{i}}$ is the spin of the iron atom at site \mathbf{i} and \mathbf{x}, \mathbf{y} are unit vectors along the axes. This spin-nematic phase has been studied analytically both in strong [5, 6, 31] and weak coupling [8]. The \mathcal{O}_{rth} -distortion $\epsilon_{\mathbf{i}}$ associated to the elastic constant C_{66} will be considered here. This distortion is produced by coupling of lattice with the short-range magnetic fluctuations via $H_{\text{SL}} = -g \sum_{\mathbf{i}} \Psi_{\mathbf{i}} \epsilon_{\mathbf{i}}$ [8, 9, 32]. Here, g is the lattice-spin coupling, $\epsilon_{\mathbf{i}}$ is the \mathcal{O}_{rth} strain

$$\epsilon_{\mathbf{i}} = \frac{1}{4\sqrt{2}} \sum_{\nu=1}^4 (|\delta_{\mathbf{i}, \nu}^y| - |\delta_{\mathbf{i}, \nu}^x|), \quad (2)$$

and $\delta_{\mathbf{i}, \nu}^x$ ($\delta_{\mathbf{i}, \nu}^y$) is the component along x (y) of the distance between the Fe atom at site \mathbf{i} of the lattice and one of its four neighboring As atoms that are labeled by the index ν [33]. In this context, if the atoms could not move, the structural distortion would not occur but the C_4 symmetry would still spontaneously break at a temperature $T^* > T_N$, leading to an anisotropic resistivity [23]. The spin in H_{SL} will only be the localized spin for computational simplicity. From the other perspective, the orbital fluctuation theory attributes the structural transition to the coupling of the lattice to the \mathcal{O}_{rth} quadrupole operator via $H_{\text{OL}} = \lambda \sum_{\mathbf{i}} \Phi_{\mathbf{i}} \epsilon_{\mathbf{i}}$. Here, λ is the orbital-lattice coupling, $\Phi_{\mathbf{i}} = n_{\mathbf{i}, xz} - n_{\mathbf{i}, yz}$ is the orbital order parameter, and $n_{\mathbf{i}, \alpha}$ the electronic density at site \mathbf{i} and orbital α [19, 20].

Finally, H_{Stiff} is

$$H_{\text{Stiff}} = \frac{1}{2} k \sum_{\mathbf{i}} \sum_{\nu=1}^4 (|\mathbf{R}_{\text{Fe-As}}^{\mathbf{i}, \nu}| - R_0)^2 + k' \sum_{\langle \mathbf{ij} \rangle} \left[\left(\frac{a_0}{R_{\text{Fe-Fe}}^{\mathbf{ij}}} \right)^{12} - 2 \left(\frac{a_0}{R_{\text{Fe-Fe}}^{\mathbf{ij}}} \right)^6 \right]. \quad (3)$$

The first term in Eq. (3) is the standard harmonic energy. The second term contains anharmonic contributions to improve the simulations' convergence [34].

Only the \mathcal{O}_{rth} -distortion is considered here since our aim is to study the structural transition of the parent compounds [20]. In equilibrium, the Fe atoms form a square lattice with sites labeled by \mathbf{i} and with lattice parameter a_0 ; the As atoms are at the center of each plaquette, identified with the indices (\mathbf{i}, ν) , with coordinate $z = \pm a_0/2$ in alternating plaquettes so that the Fe-As equilibrium distance is $R_0 = \sqrt{3}a_0/2$. In our study, each As atom is allowed to move in the $x-y$ plane to a new position $\mathbf{R}_{\text{Fe-As}}^{\mathbf{i}, \nu} = (\delta_{\mathbf{i}, \nu}^x, \delta_{\mathbf{i}, \nu}^y, \pm a_0/2)$ with respect to the Fe atom that was at site \mathbf{i} when in equilibrium. The distance between Fe atoms, $R_{\text{Fe-Fe}}^{\mathbf{ij}}$, is determined *globally* via the variables a_x and a_y , both equal to a_0 when in equilibrium, satisfying the constraints $2Na_x = \sum_{\mathbf{i}=1}^N \sum_{\nu} |\delta_{\mathbf{i}, \nu}^x|$ and $2Na_y = \sum_{\mathbf{i}=1}^N \sum_{\nu} |\delta_{\mathbf{i}, \nu}^y|$ where N is the number of sites and $\nu=1, \dots, 4$ are the four As atoms connected to each Fe. Note that this procedure is qualitatively different from studies of Jahn-Teller distortions in Mn-oxides where the Mn-Mn distance was fixed [22], while here the Fe-Fe distances can change due to the \mathcal{O}_{rth} -distortion leading to the global adjustments in lattice spacings.

The Hamiltonian is here studied via a standard MC simulation in the classical (a) localized spins $\mathbf{S}_{\mathbf{i}}$ and (b) atomic displacements $\delta_{\mathbf{i}, \nu}^x$ and $\delta_{\mathbf{i}, \nu}^y$. For each MC configuration of spins and atomic positions the fermionic quantum Hamiltonian is diagonalized via library subroutines, as extensively discussed in the manganite context [22], rendering the study computationally demanding.

Results. - The MC simulations were performed on 8×8 square clusters using “twisted boundary conditions” that effectively reduce finite size effects, as discussed before [26]. Typically 8,000 MC steps were used for thermalization and 50,000-100,000 steps for measurements at each temperature T and for each set of parameters. The Hund interaction was set to $J_{\text{H}} = 0.1$ eV, and the classical Heisenberg couplings to $J_{\text{NN}} = 0.012$ eV and $J_{\text{NNN}} = 0.008$ eV, similarly as in Ref. [26]. Fixing some parameters to values used in previous investigations simplifies the analysis and allow us to focus on the effects of the lattice into a previously studied system. The stiffness constants were selected so that the dimensionless couplings $\tilde{\lambda} = \frac{2\lambda}{kW}$ and $\tilde{g} = \frac{2g}{kW}$ [22] are experimentally realistic [35] (W =fermionic bandwidth). Calculations indicate that both parameters should be smaller than 1 in pnictides [7, 19, 20, 36]. The magnetic transition will be determined by the magnetic susceptibility

$$\chi_{S(\pi,0)} = N\beta\langle S(\pi,0) - \langle S(\pi,0) \rangle \rangle^2, \quad (4)$$

where $\beta = 1/k_B T$, N is the number of lattice sites, and $S(\pi,0)$ is the magnetic structure factor [at the wavevector $(\pi,0)$ of relevance in pnictides] obtained via the Fourier transform of the real-space spin-spin correlations measured during the simulations. The structural transition is determined by the behavior of the lattice susceptibility defined by $\chi_\delta = N\beta\langle \delta - \langle \delta \rangle \rangle^2$, where $\delta = \frac{(a_x - a_y)}{(a_x + a_y)}$.

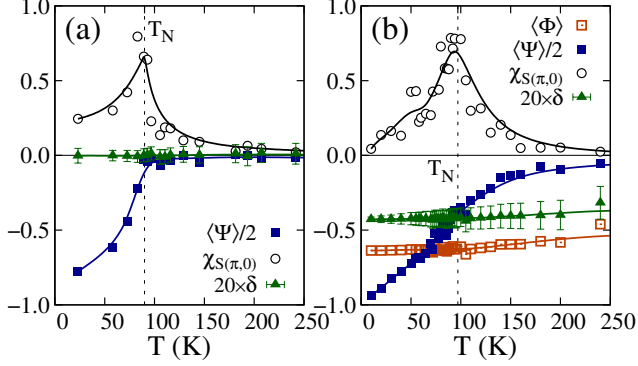


FIG. 1: (Color online) Spin magnetic susceptibility $\chi_{S(\pi,0)}$ (circles), spin-nematic order parameter $\langle \Psi \rangle$ (filled squares), and lattice distortion δ (triangles) vs. T at $\tilde{g} = 0$ and (a) $\tilde{\lambda} = 0.12$ and (b) $\tilde{\lambda} = 1.2$ (in the latter, open squares indicate orbital order). T_N is indicated by the dashed line.

Individual couplings.— To isolate the individual roles that the spin and orbital d.o.f. play in their interaction with the lattice, first the case $\tilde{g} = 0$ was studied, varying T at several values of $\tilde{\lambda}$. At $\tilde{\lambda} = 0.12$ neither a sizable lattice distortion [as indicated by the triangles in Fig. 1(a)] nor orbital order were observed, and only a Néel transition at $T_N = 90$ K into a collinear AFM $(\pi,0)$ state was found (see circles in the figure). To develop a more robust lattice distortion $\tilde{\lambda}$ must be increased to unphysical large values. In fact, numerically it was observed that varying $\tilde{\lambda}$ the orbital order and structural distortion are stabilized for $\tilde{\lambda} > 0.8$. However, in this $\tilde{\lambda}$ regime, already larger than estimations [19, 36], the \mathcal{O}_{rth} -distortion has the longest lattice constant along the FM direction (see Fig. 1(b) at $\tilde{\lambda} = 1.2$), qualitatively opposite to experimental observations [37]. As a consequence, in our model, that relies on a particular set of hopping amplitudes chosen to fit ARPES experiments, the physical \mathcal{O}_{rth} /magnetic state of pnictides cannot arise from short-range orbital fluctuations alone [20]. Let us study next the role played by the spin-lattice coupling by setting instead $\tilde{\lambda} = 0$ and focusing on, e.g., $\tilde{g} = 0.16$. In this case, a peak in χ_δ [see Fig. 2(a)] denotes a structural transition. This transition now has the experimentally correct \mathcal{O}_{rth} -distortion below T_N , i.e. $\delta > 0$, and it occurs simultaneously with the Néel transition at $T_S = T_N = 153$ K. The ordered phase now has both long-range magnetic order and a long-range \mathcal{O}_{rth} -distortion

with $\delta = (a_x - a_y)/(a_x + a_y) \approx 0.0037$ (green triangles), remarkably close to experiments suggesting that the small couplings to the lattice considered here are physically reasonable. However, setting $\tilde{\lambda} = 0$ no orbital order was observed, at least with the hopping amplitudes employed here. Moreover our study shows that T_N remains equal (within the accuracy of our effort) to T_S in the physical regime, contrary to experiments. Then, neither the limits $\tilde{\lambda} = 0$ nor $\tilde{g} = 0$ are sufficient to fully accommodate the phenomenology of the pnictides.

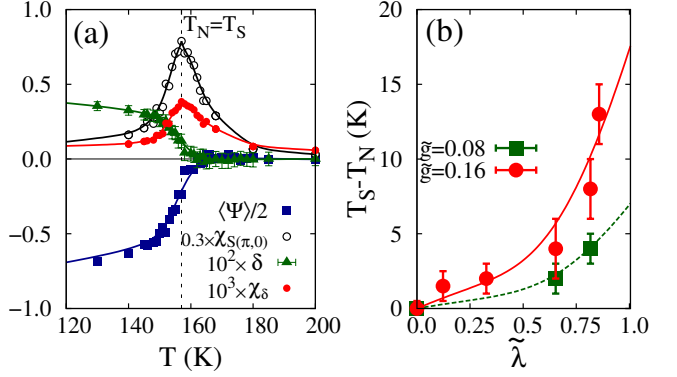


FIG. 2: (color online) (a) Spin magnetic susceptibility $\chi_{S(\pi,0)}$ (open circles), lattice distortion susceptibility χ_δ (filled circles), spin-nematic order parameter $\langle \Psi \rangle$ (squares), and lattice distortion δ (triangles) vs. T for couplings $\tilde{g} = 0.16$ and $\tilde{\lambda} = 0$. T_N and the structural transition temperature T_S are indicated by the dashed line. (b) The temperature difference between T_S and T_N vs. $\tilde{\lambda}$, at $\tilde{g} = 0.08$ and 0.16 .

Combined couplings.— Our main result is that the *combined* effect of the coupling of the lattice to both spins and orbitals is needed to reach a regime with all the characteristics of the states found experimentally in pnictides. By turning on both the spin- and orbital-lattice interactions our MC studies show that the structural transition moves to a temperature higher than the magnetic transition so that $T_S > T_N$, as shown in Fig. 2(b) at $\tilde{g} = 0.16$ and 0.08 . For small couplings in the experimental range, such as $\tilde{\lambda} = 0.12$ and $\tilde{g} = 0.16$, the difference $T_S - T_N$ is concomitantly small but it is numerically clear, with χ_δ systematically above (below) $\chi_{S(\pi,0)}$ at temperatures above (below) the critical region. More specifically, $T_N = 156$ K from the peak in χ_S (open black circles) in Fig. 3, and $T_S = 158$ K from the peak in χ_δ (filled circles). The difference in the position of the two maxima (see inset) has been extensively analyzed repeating MC runs with different starting configurations and statistics, and it appears robust. Moreover, $T_S - T_N$ can be further enhanced by increasing $\tilde{\lambda}$ [see Figs. 2(b) and 9 (Suppl. Mat.)] [38]. The intermediate phase has a broken Z_2 symmetry with short-range NN spin-spin correlations characterized by $\langle \Psi \rangle < 0$ indicating spin-nematic order (filled squares), $\delta > 0$ indicating \mathcal{O}_{rth} distortion (triangles), and $\langle \Phi \rangle > 0$ indicating orbital order (open squares).

The order of the transitions was also investigated. In

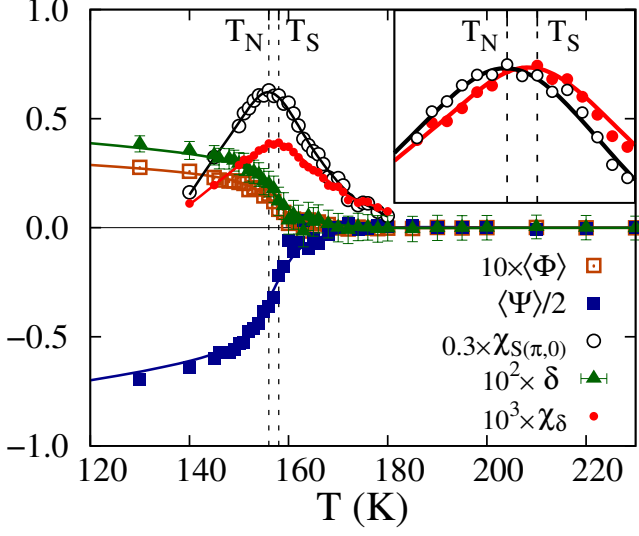


FIG. 3: (color online) Spin magnetic susceptibility $\chi_{S(\pi,0)}$ (open circles), lattice distortion susceptibility χ_δ (filled circles), spin-nematic order parameter $\langle\Psi\rangle$ (filled squares), orbital order $\langle\Phi\rangle$ (open squares), and lattice distortion δ (triangles) vs. T at couplings $\tilde{g}=0.16$ and $\tilde{\lambda}=0.12$. T_N and T_S are indicated by the dashed lines. *Inset*: close-up of the $\chi_{S(\pi,0)}$ and χ_δ peaks, shifted vertically for better comparison.

Fig. 4(a) the spin-nematic order parameter $\langle\Psi\rangle$ is shown varying T at several $\tilde{\lambda}$'s and fixed $\tilde{g}=0.16$. At small $\tilde{\lambda}$, where $T_N=T_S$ according to Fig. 2(a), the transition is abrupt as in a first-order transition. Upon increasing $\tilde{\lambda}$, leading to $T_S>T_N$, the transition becomes continuous as in a second-order transition. This is in agreement with predictions of an effective low-energy model [8].

Comparison with experiments.— As in the previous effort employing the purely electronic SF model [26] the resistance R along the AFM and FM directions was calculated varying T . While the reproduction of the uniaxial-pressure experimental results [23] required previously an explicit anisotropy in the Heisenberg couplings to mimic strain, now the asymmetry develops *spontaneously* as shown in Fig. 4(b). R along the FM direction becomes larger than along the AFM direction at $T \approx T_S$ suggesting that the anisotropy observed above T_S in experiments may be due to the external strain [39, 40].

Our study also reproduces the ARPES experiments [41–43] where an asymmetry develops between the spectral weight for the xz and yz orbitals along the $\Gamma-X$ and the $\Gamma-Y$ directions upon cooling. In Fig. 5 it is shown that along the $\Gamma-X$ [$\Gamma-Y$] direction, mainly near $(\pi,0)$ [$(0,\pi)$], the spectral weight for the yz (xz) orbital moves closer to (further from) the Fermi level as T is lowered, compatible with the development of orbital order with $\langle\Phi\rangle>0$. The asymmetry is obtained here without explicit symmetry breaking at the Hamiltonian level [44]. Note also that orbital order may only occur near the Fermi Surface [45]. It is important to re-

mark that in spite of the small values of $\tilde{\lambda}$ and \tilde{g} used in our effort, their influence is sufficient to create observable consequences such as the anisotropies in transport and ARPES. In addition, a recent pair-distribution function analysis reported the presence of robust *local* \mathcal{O}_{rth} -distortions [46], hinting that the lattice d.o.f. is more important than previously believed [47].

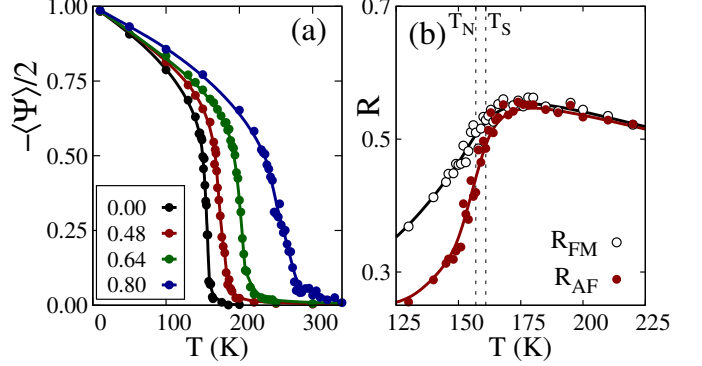


FIG. 4: (Color online) (a) Spin-nematic order parameter $\langle\Psi\rangle$ vs. T at $\tilde{g} = 0.16$ and for the values of $\tilde{\lambda}$ indicated. (b) MC resistance along the x (AFM) and y (FM) direction varying T . Dashed lines indicate T_N and T_S at $\tilde{g} = 0.16$ and $\tilde{\lambda} = 0.12$.

Conclusions.— In the model analyzed here, the couplings of the spin and orbital d.o.f. with the lattice are *both* important to stabilize the state that breaks the C_4 symmetry above the Néel transition. The spin-lattice coupling induces the correct experimentally observed \mathcal{O}_{rth} -distortion, while the orbital-lattice coupling generates the ARPES-observed orbital order and the higher temperature structural transition. As a consequence, our study suggests that the complex nematic properties of the pnictides parent compounds arise from a subtle cooperation among all the participating degrees of freedom.

Acknowledgment.— This work was supported by the U.S. Department of Energy, Office of Basic Energy Sciences, Materials Sciences and Engineering Division.

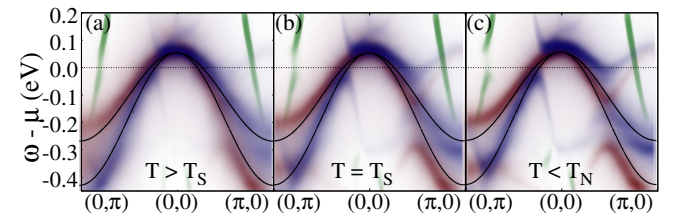


FIG. 5: (Color online) Orbital-resolved spectral weight of the SF model along the directions $(0,\pi)-(0,0)-(\pi,0)$ in momentum space for (a) $T=165$ K, (b) $T=158$ K, and (c) $T=145$ K, at $\tilde{g}=0.16$ and $\tilde{\lambda}=0.12$. The non-interacting band dispersion is indicated by the solid black lines. The spectral weight for the d_{xz} , d_{yz} , and d_{xy} orbitals is indicated by the red, blue, and green dots, respectively.

-
- [1] D. C. Johnston, Adv. Phys. **59**, 803 (2010).
- [2] P. Dai, J.-P. Hu, and E. Dagotto, Nat. Phys. **8**, 709 (2012).
- [3] R. M. Fernandes, D. K. Pratt, W. Tian, J. Zarestky, A. Kreyssig, S. Nandi, M. G. Kim, A. Thaler, N. Ni, P. C. Canfield, R. J. McQueeney, J. Schmalian, and A. I. Goldman, Phys. Rev. B **81**, 140501(R) (2010).
- [4] S. Nandi, M. G. Kim, A. Kreyssig, R. M. Fernandes, D. K. Pratt, A. Thaler, N. Ni, S. L. Bud'ko, P. C. Canfield, J. Schmalian, R. J. McQueeney, and A. I. Goldman, Phys. Rev. Lett. **104**, 057006 (2010).
- [5] C. Fang, H. Yao, W.-F. Tsai, J.P. Hu, and S. A. Kivelson, Phys. Rev. B **77**, 224509 (2008).
- [6] C. Xu, M. Müller, and S. Sachdev, Phys. Rev. B **78**, 020501(R) (2008).
- [7] R. M. Fernandes, L. H. VanBebber, S. Bhattacharya, P. Chandra, V. Keppens, D. Mandrus, M. A. McGuire, B. C. Sales, A. S. Sefat, and J. Schmalian, Phys. Rev. Lett. **105**, 157003 (2010).
- [8] R. M. Fernandes, A. V. Chubukov, J. Knolle, I. Eremin, and J. Schmalian, Phys. Rev. B **85**, 024534 (2012).
- [9] R. M. Fernandes and J. Schmalian, Supercond. Sci. Technol. **25**, 084005 (2012).
- [10] E. Fradkin, S. A. Kivelson, M. J. Lawler, J. P. Eisenstein, and A. P. Mackenzie, Annu. Rev. Cond. Mat. Phys. **1**, 153 (2010).
- [11] Y. Kamiya, N. Kawashima, and C. D. Batista, Phys. Rev. B **84**, 214429 (2011).
- [12] A. L. Wysocki, K. D. Belashchenko, and V. P. Antropov, Nat. Phys. **7**, 485 (2011).
- [13] S. Kasahara, H.J. Shi, K. Hashimoto, S. Tonegawa, Y. Mizukami, T. Shibauchi, K. Sugimoto, T. Fukuda, T. Terashima, A. H. Nevidomskyy, and Y. Matsuda, Nature **486**, 382 (2012).
- [14] A. F. Wang *et al.*, arXiv:1207.3852.
- [15] C.-C. Lee, W.-G. Yin, and Wei Ku, Phys. Rev. Lett. **103**, 267001 (2009).
- [16] C.-C. Chen, B. Moritz, J. van den Brink, T. P. Devereaux, and R. R. P. Singh, Phys. Rev. B **80**, 180418(R) (2009).
- [17] W. Lv, J.S. Wu, and P. Phillips, Phys. Rev. B **80**, 224506 (2009).
- [18] C.-C. Chen, J. Maciejko, A. P. Sorini, B. Moritz, R. R. P. Singh, and T. P. Devereaux, Phys. Rev. B **82**, 100504(R) (2010).
- [19] H. Kontani, Y. Inoue, T. Saito, Y. Yamakawa, and S. Onari, Solid State Comm. **152**, 718 (2012).
- [20] H. Kontani, T. Saito, and S. Onari, Phys. Rev. B **84**, 024528 (2011).
- [21] W.-C. Lee, W. Lv, J. M. Tranquada, and P. W. Phillips, Phys. Rev. B **86**, 094516 (2012).
- [22] E. Dagotto, T. Hotta, and A. Moreo, Phys. Rep. **344**, 1 (2001).
- [23] J.-H. Chu, J. G. Analytis, K. De Greve, P. L. McMahon, Z. Islam, Y. Yamamoto, and I. R. Fisher, Science **329**, 824 (2010); See also I. R. Fisher, L. Degiorgi, and Z. X. Shen, Rep. Prog. Phys. **74**, 124506 (2011).
- [24] W. Lv, F. Krüger, and P. Phillips, Phys. Rev. B **82**, 045125 (2010).
- [25] W.-G. Yin, C.-C. Lee, and W. Ku, Phys. Rev. Lett. **105**, 107004 (2010).
- [26] S. Liang, G. Alvarez, C. Sen, A. Moreo, and E. Dagotto, Phys. Rev. Lett. **109**, 047001 (2012).
- [27] H. Gretarsson *et al.*, Phys. Rev. B **84**, 100509(R) (2011).
- [28] F. Bondino *et al.*, Phys. Rev. Lett. **101**, 267001 (2008).
- [29] M. Daghofer, A. Nicholson, A. Moreo, and E. Dagotto, Phys. Rev. B **81**, 014511 (2010).
- [30] J. L. Niedziela, D. Parshall, K. A. Lokshin, A. S. Sefat, A. Alatas, and T. Egami, Phys. Rev. B **84**, 224305 (2011).
- [31] Q. Si and E. Abrahams, Phys. Rev. Lett. **101**, 076401 (2008).
- [32] J.-H. Chu, H.-H. Kuo, J.G. Analytis, and I. R. Fisher, Science **337**, 710 (2012).
- [33] According to the experimental results it is known that $\langle \epsilon_i \rangle < 0$ if the magnetic order of the ground state is $(\pi, 0)$ [23]. For this reason only positive values of the spin-lattice constant g must be considered since otherwise an unphysical lattice distortion would result.
- [34] If only harmonic terms are considered for the Fe atoms the results do not change but it takes longer to achieve numerical convergence.
- [35] $W=3$ eV is the bandwidth of the three-orbital model [29].
- [36] L. Boeri, O. V. Dolgov, and A. A. Golubov, Phys. Rev. Lett. **101**, 026403 (2008).
- [37] If in the orbital-lattice term H_{OL} a negative value of ϵ is introduced and kept fixed, so that $a_x > a_y$ as in experiments, a distortion of the FS that favors the intra-orbital nesting along $(0, \pi)$ is induced. Thus, changing the sign of the coupling in H_{OL} leads to the correct lattice distortion but the incorrect spin order.
- [38] Integrating out the lattice d.o.f. in our model may lead to the 3-point vertex couplings discussed by S. Onari and H. Kontani, Phys. Rev. Lett. **109**, 137001 (2012), where $T_S > T_N$ is also reported.
- [39] C. Dhital, Z. Yamani, Wei Tian, J. Zeretsky, A. S. Sefat, Ziqiang Wang, R. J. Birgeneau, and S. D. Wilson, Phys. Rev. Lett. **108**, 087001 (2012).
- [40] E. C. Blomberg, A. Kreyssig, M.A. Tanatar, R.M. Fernandes, M. G. Kim, A. Thaler, J. Schmalian, S. L. Bud'ko, P. C. Canfield, A. I. Goldman, and R. Prozorov, Phys. Rev. B **85**, 144509 (2012).
- [41] M. Yi, D. H. Lu, J.-H. Chu, J. G. Analytis, A. P. Sorini, A. F. Kemper, S.-K. Mo, R. G. Moore, M. Hashimoto, W. S. Lee, Z. Hussain, T. P. Devereaux, I. R. Fisher, and Z.-X. Shen, Proc. Natl. Acad. Sci. USA **108**, 6878 (2011).
- [42] C. He, Y. Zhang, B. P. Xie, X. F. Wang, L. X. Yang, B. Zhou, F. Chen, M. Arita, K. Shimada, H. Namatame, M. Taniguchi, X. H. Chen, J. P. Hu, and D. L. Feng, Phys. Rev. Lett. **105**, 117002 (2010).
- [43] Y. Zhang *et al.*, Phys. Rev. B **85**, 085121 (2012).
- [44] M. Daghofer, A. Nicholson, and A. Moreo, Phys. Rev. B **85**, 184515 (2012).
- [45] M. Daghofer, Q.-L. Luo, R. Yu, D. X. Yao, A. Moreo, and E. Dagotto, Phys. Rev. B **81**, 180514(R) (2010).
- [46] J. L. Niedziela, M. A. McGuire, and T. Egami, Phys. Rev. B **86**, 174113 (2012).
- [47] Similar conclusions were reached in a recent ARPES study of $\text{Fe}_{1.02}\text{Te}$: Z.K. Liu, R.H. He, D.H. Lu, Ming Yi, Yulin Chen, M. Hashimoto, R. G. Moore, S.-K. Mo, E. A. Nowadnick, Jin Hu, T.J. Liu, Z.Q. Mao, T. P. Devereaux, Z. Hussain, and Z.-X. Shen, arXiv:1212.4946.
- [48] J. Salafranca, G. Alvarez, and E. Dagotto, Phys. Rev. B **80**, 155133 (2009).
- [49] Y. Ono, Y. Yanagi, N. Adachi, and Y. Yamakawa, Solid

SUPPLEMENTARY MATERIAL

Full Hamiltonian

The full Hamiltonian of the spin-fermion model with lattice interactions incorporated is given by:

$$H_{\text{SF}} = H_{\text{Hopp}} + H_{\text{Hund}} + H_{\text{Heis}} + H_{\text{SL}} + H_{\text{OL}} + H_{\text{Stiff}}. \quad (5)$$

The hopping component is made of three contributions,

$$H_{\text{Hopp}} = H_{xz,yz} + H_{xy} + H_{xz,yz;xy}. \quad (6)$$

The first term involves the xz and yz orbitals as follows:

$$\begin{aligned} H_{xz,yz} = & \{ -t_1 \sum_{\mathbf{i},\sigma} (d_{\mathbf{i},xz,\sigma}^\dagger d_{\mathbf{i}+\hat{y},xz,\sigma} + d_{\mathbf{i},yz,\sigma}^\dagger d_{\mathbf{i}+\hat{x},yz,\sigma}) \\ & - t_2 \sum_{\mathbf{i},\sigma} (d_{\mathbf{i},xz,\sigma}^\dagger d_{\mathbf{i}+\hat{x},xz,\sigma} + d_{\mathbf{i},yz,\sigma}^\dagger d_{\mathbf{i}+\hat{y},yz,\sigma}) \\ & - t_3 \sum_{\mathbf{i},\hat{\mu} \neq \hat{\nu},\sigma} (d_{\mathbf{i},xz,\sigma}^\dagger d_{\mathbf{i}+\hat{\mu}+\hat{\nu},xz,\sigma} + d_{\mathbf{i},yz,\sigma}^\dagger d_{\mathbf{i}+\hat{\mu}+\hat{\nu},yz,\sigma}) \\ & + t_4 \sum_{\mathbf{i},\sigma} (d_{\mathbf{i},xz,\sigma}^\dagger d_{\mathbf{i}+\hat{x}+\hat{y},yz,\sigma} + d_{\mathbf{i},yz,\sigma}^\dagger d_{\mathbf{i}+\hat{x}+\hat{y},xz,\sigma}) \\ & - t_4 \sum_{\mathbf{i},\sigma} (d_{\mathbf{i},xz,\sigma}^\dagger d_{\mathbf{i}+\hat{x}-\hat{y},yz,\sigma} + d_{\mathbf{i},yz,\sigma}^\dagger d_{\mathbf{i}+\hat{x}-\hat{y},xz,\sigma}) \\ & + h.c. \} - \mu \sum_{\mathbf{i}} (n_{\mathbf{i},xz} + n_{\mathbf{i},yz}). \end{aligned} \quad (7)$$

The second term contains the hoppings related with the xy orbital:

$$\begin{aligned} H_{xy} = & t_5 \sum_{\mathbf{i},\hat{\mu},\sigma} (d_{\mathbf{i},xy,\sigma}^\dagger d_{\mathbf{i}+\hat{\mu},xy,\sigma} + h.c.) \\ & - t_6 \sum_{\mathbf{i},\hat{\mu} \neq \hat{\nu},\sigma} (d_{\mathbf{i},xy,\sigma}^\dagger d_{\mathbf{i}+\hat{\mu}+\hat{\nu},xy,\sigma} + h.c.) \\ & + \Delta_{xy} \sum_{\mathbf{i}} n_{\mathbf{i},xy} - \mu \sum_{\mathbf{i}} n_{\mathbf{i},xy}, \end{aligned} \quad (8)$$

TABLE I: Values of the parameters that appear in the tight-binding portion of the three-orbital model Eqs.(7) to (9). The overall energy unit is electron volts.

t_1	t_2	t_3	t_4	t_5	t_6	t_7	t_8	Δ_{xy}
0.02	0.06	0.03	-0.01	0.2	0.3	-0.2	0.1	0.4

Finally, the last term contributing to the hopping is:

$$\begin{aligned} H_{xz,yz;xy} = & -t_7 \sum_{\mathbf{i},\sigma} [(-1)^{|\mathbf{i}|} d_{\mathbf{i},xz,\sigma}^\dagger d_{\mathbf{i}+\hat{x},xy,\sigma} + h.c.] \\ & - t_7 \sum_{\mathbf{i},\sigma} [(-1)^{|\mathbf{i}|} d_{\mathbf{i},xy,\sigma}^\dagger d_{\mathbf{i}+\hat{x},xz,\sigma} + h.c.] \\ & - t_7 \sum_{\mathbf{i},\sigma} [(-1)^{|\mathbf{i}|} d_{\mathbf{i},yz,\sigma}^\dagger d_{\mathbf{i}+\hat{y},xy,\sigma} + h.c.] \\ & - t_7 \sum_{\mathbf{i},\sigma} [(-1)^{|\mathbf{i}|} d_{\mathbf{i},xy,\sigma}^\dagger d_{\mathbf{i}+\hat{y},yz,\sigma} + h.c.] \\ & - t_8 \sum_{\mathbf{i},\sigma} [(-1)^{|\mathbf{i}|} d_{\mathbf{i},xz,\sigma}^\dagger d_{\mathbf{i}+\hat{x}+\hat{y},xy,\sigma} + h.c.] \\ & + t_8 \sum_{\mathbf{i},\sigma} [(-1)^{|\mathbf{i}|} d_{\mathbf{i},xy,\sigma}^\dagger d_{\mathbf{i}+\hat{x}+\hat{y},xz,\sigma} + h.c.] \\ & - t_8 \sum_{\mathbf{i},\sigma} [(-1)^{|\mathbf{i}|} d_{\mathbf{i},xz,\sigma}^\dagger d_{\mathbf{i}+\hat{x}-\hat{y},xy,\sigma} + h.c.] \\ & + t_8 \sum_{\mathbf{i},\sigma} [(-1)^{|\mathbf{i}|} d_{\mathbf{i},xy,\sigma}^\dagger d_{\mathbf{i}+\hat{x}-\hat{y},yz,\sigma} + h.c.] \\ & - t_8 \sum_{\mathbf{i},\sigma} [(-1)^{|\mathbf{i}|} d_{\mathbf{i},yz,\sigma}^\dagger d_{\mathbf{i}+\hat{x}+\hat{y},xy,\sigma} + h.c.] \\ & + t_8 \sum_{\mathbf{i},\sigma} [(-1)^{|\mathbf{i}|} d_{\mathbf{i},xy,\sigma}^\dagger d_{\mathbf{i}+\hat{x}+\hat{y},yz,\sigma} + h.c.] \\ & + t_8 \sum_{\mathbf{i},\sigma} [(-1)^{|\mathbf{i}|} d_{\mathbf{i},yz,\sigma}^\dagger d_{\mathbf{i}+\hat{x}-\hat{y},xy,\sigma} + h.c.] \\ & - t_8 \sum_{\mathbf{i},\sigma} [(-1)^{|\mathbf{i}|} d_{\mathbf{i},xy,\sigma}^\dagger d_{\mathbf{i}+\hat{x}-\hat{y},yz,\sigma} + h.c.]. \end{aligned} \quad (9)$$

In the equations shown above, the operator $d_{\mathbf{i},\alpha,\sigma}^\dagger$ creates an electron at site \mathbf{i} of the two-dimensional lattice of irons. The orbital index is $\alpha = xz, yz$, or xy , and the z -axis spin projection is denoted by σ . The chemical potential used to regulate the electronic density is μ . The symbols \hat{x} and \hat{y} denote vectors along the axes that join NN atoms. The values of the hoppings t_i were discussed originally in Ref. [29] and for the benefit of the readers they are reproduced here in Table I, including also the value of the energy splitting Δ_{xy} .

The remaining terms of the Hamiltonian have been presented in the main text, but they are reproduced below again for completeness. The symbols $\langle \rangle$ denote NN while $\langle\langle \rangle\rangle$ denote NNN. The rest of the notation was already explained in the main text.

$$H_{\text{Hund}} = -J_{\text{H}} \sum_{\mathbf{i},\alpha} \mathbf{S}_{\mathbf{i}} \cdot \mathbf{S}_{\mathbf{i},\alpha}, \quad (10)$$

$$H_{\text{Heis}} = J_{\text{NN}} \sum_{\langle \mathbf{ij} \rangle} \mathbf{S}_i \cdot \mathbf{S}_j + J_{\text{NNN}} \sum_{\langle \langle \mathbf{im} \rangle \rangle} \mathbf{S}_i \cdot \mathbf{S}_m, \quad (11)$$

$$H_{\text{SL}} = -g \sum_i \Psi_i \epsilon_i, \quad (12)$$

$$H_{\text{OL}} = \lambda \sum_i \Phi_i \epsilon_i, \quad (13)$$

$$H_{\text{Stiff}} = \frac{1}{2} k \sum_i \sum_{\nu=1}^4 (|\mathbf{R}_{Fe-As}^{i\nu}| - R_0)^2 + k' \sum_{\langle \mathbf{ij} \rangle} \left[\left(\frac{a_0}{R_{Fe-Fe}^{ij}} \right)^{12} - 2 \left(\frac{a_0}{R_{Fe-Fe}^{ij}} \right)^6 \right]. \quad (14)$$

Lattice Distortions

The definition of the lattice variables used in our calculations is shown in Fig. 6. Panel (a) indicates the equilibrium position of the Fe atoms at the sites \mathbf{i} of a square lattice, with equilibrium lattice constants $a_x = a_y = a_0$. In equilibrium, namely without the influence of the electronic degrees of freedom, the As atoms are separated by $a_0/2$ from each Fe with regards to their x and y axes coordinates, while they are at distance $a_0/2$ above or below the $x-y$ plane on alternating plaquettes (remember the As atoms are not in the same plane as the Fe atoms). During the Monte Carlo simulation the As atoms are allowed to move *locally* away from their equilibrium positions but with movements restricted to be only along the x and y directions for simplicity. The Fe atoms, on the other hand, can only move *globally* also along the x (y) direction [see panel (a) of Fig. 7] such that the inter-Fe distance a_x (a_y) arises from the constraint $2Na_r = \sum_{i=1}^N \sum_{\nu} |\delta_{i,\nu}^r|$. In this formula $r = x, y$, N is the number of sites of the lattice, and $\delta_{i,\nu}^r$ is the component along the r axis of the distance between the Fe atom at site \mathbf{i} and one of the As atoms in the neighboring plaquette. The four As neighbors to a given Fe are labeled by the index $\nu = 1, \dots, 4$. The equilibrium values of $\delta_{i,\nu}^r$ are shown in panel (b) of Fig. 6 while non-equilibrium values are shown in panel (b) of Fig. 7. In the latter, the atomic equilibrium positions are shown in black and the non-equilibrium positions in red.

The \mathcal{O}_{rth} strain ϵ_i defined in Eq. 2 is schematically shown in panel (b) of Fig. 8 where the displacements $\delta_{i,\nu}^r$'s at site \mathbf{i} are shown for $r = x, y$ and $\nu = 1, 2, 3, 4$, while panel (a) depicts the undistorted lattice as reference.

Monte Carlo Technique

The Monte Carlo technique used here to study the spin-fermion model defined in Eq. 1 is standard and

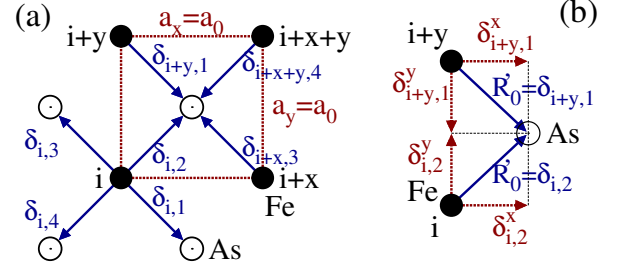


FIG. 6: (color online) (a) Schematic representation of the equilibrium positions of the Fe-As lattice (projected on the $x-y$ plane). Four Fe atoms are indicated with filled circles and labeled by their site index \mathbf{i} (with \mathbf{x} and \mathbf{y} being unit vectors along the axes). The open circles indicate the projection of the equilibrium position of the As ions in the $x-y$ plane. The distance between an Fe atom at site \mathbf{i} and its four neighboring As atoms is indicated by $\delta_{i,\nu}$ with ν running from 1 to 4 as shown (blue arrows). In equilibrium, $\delta_{i,\nu} = R'_0 = \sqrt{2}a_0/2$ where R'_0 is the projection on the $x-y$ plane of R_0 , the equilibrated Fe-As distance. The red dashed lines indicate the case $a_x = a_y = a_0$, namely the equilibrium distance between neighboring Fe atoms. (b) Schematic representation of the variables $\delta_{i,\nu}^x$ and $\delta_{i,\nu}^y$ (red arrows) for the case $(\mathbf{i}, 2)$ and $(\mathbf{i} + \mathbf{y}, 1)$ in the equilibrium configuration.

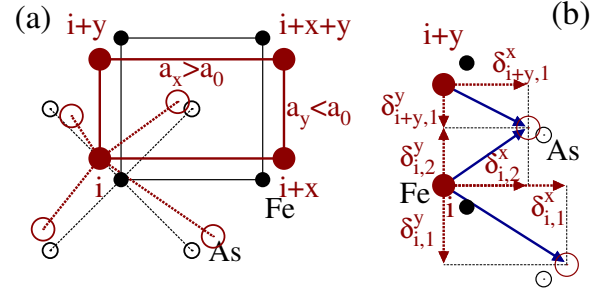


FIG. 7: (color online) (a) Schematic representation of a non-equilibrium position of the Fe-As lattice (projected on the $x-y$ plane). Four Fe atoms are indicated with red filled circles and labeled by their site index \mathbf{i} (with \mathbf{x} and \mathbf{y} being unit vectors along the axes). The red open circles indicate the projection on the $x-y$ plane of the non-equilibrium position of the As atoms. The distance between neighboring Fe atoms is a_x (a_y) along x (y) indicated by red lines. The red dashed lines show $R_{Fe-As}^{i\nu}$, which is the projection on the plane $x-y$ of the Fe-As distance $R_{Fe-As}^{i\nu}$. The equilibrium position of the atoms is indicated by the black symbols. (b) Schematic representation of the variables $\delta_{i,\nu}^x$ and $\delta_{i,\nu}^y$ (red arrows) for $(\mathbf{i}, 1)$, $(\mathbf{i}, 2)$, and $(\mathbf{i} + \mathbf{y}, 1)$ in an out-of-equilibrium configuration. The variables $\delta_{i,\nu}^x$ and $\delta_{i,\nu}^y$ are the x and y components of the distance between Fe and As atoms, $R_{Fe-As}^{i\nu}$, between the non-equilibrium position of the Fe atom at site \mathbf{i} (filled red circle) and the As atom labeled by (\mathbf{i}, ν) (open red circle). The corresponding equilibrium positions are indicated by the black symbols.

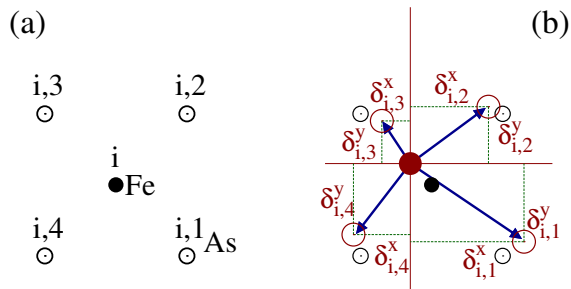


FIG. 8: (color online) (a) Schematic representation of the equilibrium position of the Fe atom at lattice site \mathbf{i} (filled circle) surrounded by the four As atoms at their equilibrium positions on the $x-y$ plane labeled by the index $\nu = 1, 2, 3, 4$. (b) Schematic representation of the variables $\delta_{i,\nu}^x$ and $\delta_{i,\nu}^y$ that define the x and y components of the distance between the non-equilibrium position of the Fe atom at site \mathbf{i} (filled red circle) and its four neighboring As atoms (open red circles). The corresponding equilibrium positions are indicated by the black symbols.

it has been extensively discussed in previous publications [22, 26] that can be consulted by the reader for more details. In this technique, the acceptance-rejection MC steps are carried out visiting the classical spins one by one and the classical lattice degrees of freedom also one by one. At each of these steps a full diagonalization of the fermionic hopping term H_{Hopp} in the background of the classical spin and lattice d.o.f. is carried out via library subroutines to calculate the energy that enters in the Metropolis algorithm. This frequent diagonalization renders the technique rather time consuming. For this reason the simulation is here limited to 8×8 clusters. For the MC time evolution, the previously described Hamiltonian H_{SF} is used with periodic boundary conditions. However, for the measurement of observables “twisted boundary conditions” (TBC) are employed [48]. In the case of TBC the classical spin and lattice configurations are assumed replicated in space with a difference of a phase factor such that a better resolution is achieved with regards to the wavevector \mathbf{k} . The reason is that a larger lattice (the replicated one) contains more eigenstates and gives a more continuous distribution of eigenvalues, reducing size-effects. In practice, TBC are introduced via phase factors ϕ that are added in the hopping amplitudes, schematically denoted by t (in reality, there are several different hopping amplitudes connecting NN and NNN Fe sites and their several orbitals, but for all of

them the same phase factor must be used). The TBC amounts to replacing t by $e^{i\phi}t$, with $\phi = 2\pi m/M$ where $m = 0, 1, \dots, M-1$ and the number of possible wavevectors in the x or y directions becomes $L = 8 \times M$.

Parameter values

In this subsection, the actual values of the parameters used in the Hamiltonian Eq. 1 are discussed. The dimensionless orbital-lattice (spin-lattice) coupling is given by $\tilde{\lambda} = \frac{\lambda}{\sqrt{kt}}$ ($\tilde{g} = \frac{g}{\sqrt{kt}}$), where t is an effective hopping related to the bandwidth W so that $t \approx W/4$. As a consequence, here it will be used $\tilde{\lambda} = \frac{2\lambda}{\sqrt{kW}}$ ($\tilde{g} = \frac{2g}{\sqrt{kW}}$) with $W=3$ eV which is the bandwidth for the three-orbital model [29]. The estimation of $\tilde{\lambda}$ in previous literature ranges from 0.1 to 0.8 [19, 36, 49]. Values in the range $\tilde{\lambda} = 2\lambda/\sqrt{kW} = 0 - 1.2$ have been used here, with the largest value only employed to highlight the incorrect lattice distortion obtained in that limit. In our MC study a small value of $\tilde{\lambda}$ approximately 0.1 is needed to observe a nonzero difference between T_N and T_S within our numerical resolution.

The spin-lattice coupling has been estimated to be $\tilde{g} = 0.002 - 1$ in the literature [7, 20]. In Ref. 20, $g_{66}/C_{66,0} = g^2/k = 0.12 - 0.21$ eV. Then $\tilde{g} = \sqrt{g_{66}/t}$. If $t \approx 0.2$ eV, then $\tilde{g} \approx 0.2 - 1$. But note that $g_{66} = 3.4 \times 10^{-6}$ eV according to Ref. 7 indicating $\tilde{g} \approx 0.004$, i.e., in previous efforts a wide range for the spin-lattice coupling has been discussed.

Determination of T_N and T_S

To determine the values of T_S and T_N extensive MC simulations and measurements of the magnetic and lattice susceptibilities, χ_S and χ_δ , were performed because of the small difference between these critical temperatures at small values of the couplings to the lattice. In the four panels of Fig. 9 the susceptibilities that allowed us to determine the values for $T_S - T_N$ at the particular coupling $\tilde{g} = 0.16$ are presented [see Fig. 2(b)]. Since at couplings such as $\tilde{\lambda}=0.8$ the difference between the critical temperatures is clear, that give us confidence that in the region of smaller $\tilde{\lambda}$'s the results are reliable since the difference $T_S - T_N$ can be followed with continuity from large $\tilde{\lambda}$ to small $\tilde{\lambda}$.

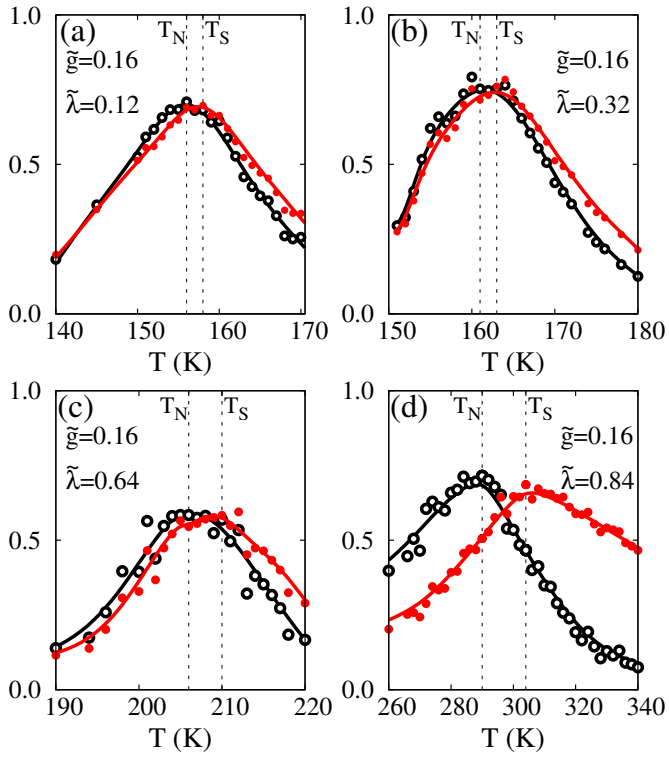


FIG. 9: (color online) T_S and T_N determined by susceptibility measurements during the Monte Carlo simulations. All results are at the couplings $\tilde{g} = 0.16$. The different panels correspond to (a) $\tilde{\lambda} = 0.12$, (b) $\tilde{\lambda} = 0.32$, (c) $\tilde{\lambda} = 0.64$, and (d) $\tilde{\lambda} = 0.84$. The results in red (solid) points are for the lattice susceptibility χ_δ . The results in black (open) points are for the spin susceptibility $\chi_{S(\pi,0)}$.